16th World Congress in Computational Mechanics (WCCM)
21-26 July 2024, Vancouver, Canada
A. Korobenko, M. Laforest, S. Prudhomme, R. Vaziri (Eds)

A FINITE DEFORMATION MICROPOLAR PERIDYNAMIC THEORY AND ITS APPLICATION TO METAMATERIALS

SAJAL[1], PRANESH ROY[2]

[1]Department of Civil Engineering, Indian Institute of Technology (Indian School of Mines) Dhanbad, Sardar Patel Nagar, Dhanbad, Jharkhand 826004, India
sajal12.20dr0122@cve.iitism.ac.in

[2]Department of Civil Engineering, Indian Institute of Technology (Indian School of Mines) Dhanbad, Sardar Patel Nagar, Dhanbad, Jharkhand 826004, India
pranesh@iitism.ac.in

Key words: Peridynamics, Micropolar, Metamaterial

Abstract. *Metamaterials with engineered microstructures exhibit exceptional properties such as negative Poisson's ratio, energy absorption, and bandgap. These materials can prevent propagation of elastic waves in certain range of frequency called bandgap. The microstructure of these materials affects the overall response of the structures. Microstructures may undergo significant rotations and their rotary inertia needs to be considered along with deformation. As the metamaterials in the study involve cracks, we develop a finite deformation micropolar peridynamics (PD) theory. The proposed PD micropolar theory is validated by comparing the results obtained from the boundary element solutions of plate with a hole. The response of metamaterials with periodic arrangement of holes and cracks is studied under static and dynamic loads and the results are compared with the nonpolar PD theory.*

1 INTRODUCTION

Metamaterials are materials with artificially engineered microstructures which can achieve exceptional material properties, e.g., auxetic behavior, high energy absorption capacity etc. Researchers developed various novel unit cell configurations to absorb elastic energy and create frequency bandgap. Golub et al. [1] observed that cracks act as reflectors of elastic waves. Sajal and Roy [2] showed the application of metamaterials with cracks for wave isolation. The microstructure of these materials affects the overall response of the structures. Microstructures may undergo significant rotations. Therefore, it is important to consider their rotary inertia along with deformation. Micropolar continuum theory is developed to address this issue that considers microrotation independent of displacement degree of freedom (Pietraszkiewicz and Eremeyev [3]). It considers the effect of microstructure by defining micro-rotation to each material point. However, micropolar theory is not suitable to analyze discontinuities as it involves partial differential governing equations. Peridynamics (PD), on the other hand, is a nonlocal continuum theory. It has integro-differential governing equations which can handle discontinuities in material bodies (Silling [4]).

We propose a finite deformation micropolar theory in non-ordinary state-based PD (NOSB-

PD) framework by postulating equations of motion. The classical micropolar material model is implemented in NOSB-PD setup using the constitutive correspondence technique developed by Silling et al. [5]. The zero-energy modes correction is applied considering the bond associated deformation gradient tensor over the intersected horizon of two material points as formulated by Chen and Spencer [6]. The solution of the governing equations for quasi-static case is obtained using the Newton-Raphson method. The Newmark-beta method is employed together with the Newton-Raphson method for dynamics case. The merit of the proposed NOSB-PD micropolar theory is demonstrated by showing the difference in response of metamaterials obtained from micropolar and nonpolar formulations in NOSB-PD.

2 FINITE DEFORMATION MICROPOLAR PD THEORY

Silling [4] proposed the PD theory which is suitable for problems dealing with cracks or discontinuities. In PD, body domain is discretized into material points with grid spacing (Δx), each representing an infinitesimally small volume. The material points interact over finite distance. For instance, as shown in Figure 1, the material point with position vector $\mathbf{x}$ in the undeformed configuration (B) interacts with a neighboring point with position vector $\mathbf{x}'$ through bond vector $\boldsymbol{\xi} = \mathbf{x}' - \mathbf{x}$. The interaction happens within a finite neighborhood $H_{\mathbf{x}}$ called horizon of $\mathbf{x}$. $H_{\mathbf{x}}$ is defined as $H_{\mathbf{x}} = \{\mathbf{x}' : |\boldsymbol{\xi}| < \delta\}$. Here δ is the radius of horizon and is considered $3.015\Delta x$ for all the simulations. Once the force is applied, the material points $\mathbf{x}$ and $\mathbf{x}'$ displace by $\mathbf{u}$ and $\mathbf{u}'$ to deformed positions vectors $\mathbf{y} = \mathbf{x} + \mathbf{u}$ and $\mathbf{y}' = \mathbf{x}' + \mathbf{u}'$ in the current configuration (B_c).

NOSB-PD is the most general form of PD theory. In NOSB-PD, direction of the force density vector state (**T**) is not restricted and can be along any direction whereas in other versions of PD, the direction of **T** is restricted to be along the direction of deformed bond.

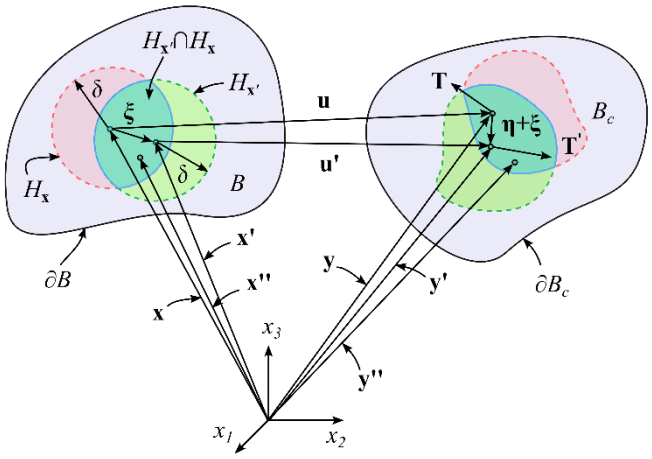

Figure 1. NOSB-PD: Reference and current configuration.

Governing equation of motion in NOSB-PD is given by

$$\rho\ddot{\mathbf{u}}(\mathbf{x},t) = \int_{H_{\mathbf{x}}} (\mathbf{T}[\mathbf{x}]\langle\boldsymbol{\xi}\rangle - \mathbf{T}[\mathbf{x}']\langle-\boldsymbol{\xi}\rangle) dV_{\mathbf{x}'} + \mathbf{b}(\mathbf{x},t), \tag{1}$$

where ρ is the mass density and $\mathbf{b}$ is the body force density vector. The notation $\mathbf{T}[\mathbf{x}]\langle\boldsymbol{\xi}\rangle$ implies that force density vector (**T)** is evaluated at material point **x** and acting on the bond $\boldsymbol{\xi}$. **T** is expressed as

$$\mathbf{T} = w(|\boldsymbol{\xi}|)\mathbf{P}(\mathbf{F})\mathbf{K}^{-1}\boldsymbol{\xi} \tag{2}$$

Here w is the influence function and **P** is the first Piola-Kirchhoff stress tensor. $w(|\boldsymbol{\xi}|) = \frac{\delta^2}{\|\boldsymbol{\xi}\|^2}$ is considered in the present study. The nonlocal deformation gradient tensor (**F**) is defined as [5]

$$\mathbf{F} = \int_{H_\mathbf{x}} (\mathbf{y}' - \mathbf{y}) \otimes \mathbf{g} dV_{\mathbf{x}'} \tag{3}$$

where $\mathbf{g} = w\mathbf{K}^{-1}\boldsymbol{\xi}$ and shape tensor, $\mathbf{K} = \int_{H_\mathbf{x}} w(|\boldsymbol{\xi}|)(\boldsymbol{\xi} \otimes \boldsymbol{\xi}) dV_{\mathbf{x}'}$. A correction is applied to **F** for elimination of zero energy deformation modes by modifying the domain $H_\mathbf{x}$ to $H_\mathbf{x} \cap H_{\mathbf{x}'}$ and expressed as [5,6]

$$\mathbf{F}_{\boldsymbol{\xi}} = \int_{H_\mathbf{x} \cap H_{\mathbf{x}'}} (\mathbf{y}'' - \mathbf{y}) \otimes \mathbf{g}_{\boldsymbol{\xi}\boldsymbol{\zeta}} dV_{\mathbf{x}''} \tag{4}$$

Here $\mathbf{g}_{\boldsymbol{\xi}\boldsymbol{\zeta}} = w(|\boldsymbol{\xi}|)\mathbf{K}_{\boldsymbol{\xi}}^{-1}\boldsymbol{\zeta}$ with $\boldsymbol{\zeta} = \mathbf{x}'' - \mathbf{x}$. $\mathbf{K}_{\boldsymbol{\xi}}$ is defined as $\mathbf{K}_{\boldsymbol{\xi}} = \int_{H_\mathbf{x} \cap H_{\mathbf{x}'}} w(|\boldsymbol{\xi}|)(\boldsymbol{\zeta} \otimes \boldsymbol{\zeta}) dV_{\mathbf{x}''}$. After the zero-energy correction, $\mathbf{T} = w(|\boldsymbol{\xi}|)\mathbf{P}(\mathbf{F}_{\boldsymbol{\xi}})\mathbf{K}^{-1}\boldsymbol{\xi}$.

In micropolar continuum, equations of motion are given as [3]

$$\nabla \cdot \mathbf{P} + \mathbf{b} = \rho\ddot{\mathbf{y}} \tag{5}$$

$$\nabla \cdot \mathbf{M} - ax(\mathbf{F}\mathbf{P}^{\mathrm{T}} - \mathbf{P}\mathbf{F}^{\mathrm{T}}) + \mathbf{l} = \dot{\mathbf{H}} \tag{6}$$

where **M**, $\boldsymbol{l}$, and **H** represent the couple stress tensor, body moment density vector, and spin angular momentum density pseudovector, respectively. **H** is given by: $\mathbf{H} = \mathbf{I}_p\boldsymbol{w}$, where $\mathbf{I}_p$ denotes the mass moment of inertia density tensor which varies with the internal microstructure and **w** is the angular velocity. The notation $ax(\cdot)$ in Eq. (6) signifies the axial vector of a skew-symmetric tensor.

Equations of motion for finite deformation micropolar PD theory are postulated as (Sajal and Roy [7])

$$\rho\ddot{\mathbf{y}} = \int_{H_\mathbf{x}} (\mathbf{T} - \mathbf{T}') dV' + \mathbf{b} \tag{7}$$

$$\dot{\mathbf{H}} = \int_{H_\mathbf{x}} (\mathbf{m} - \mathbf{m}') dV' - \int_{H_\mathbf{x}} (\mathbf{y} - \mathbf{y}') \times \mathbf{T} dV' + \mathbf{l} \tag{8}$$

Using the constitutive correspondence technique proposed by Silling et al. [5], following relation is obtained between PD and classical constitutive equations:

$$\mathbf{T} = \mathbf{P}\mathbf{g} \tag{9}$$

$$\mathbf{m} = \mathbf{M}\mathbf{g} \tag{10}$$

Extending the constitutive model for a homogeneous, isotropic, centro-symmetric, and hyperelastic micropolar material proposed by Nowacki [8], and using nonlocal versions of the strain (**E**) and wryness ($\bar{\boldsymbol{\Gamma}}$) measures, we obtain:

$$\bar{\mathbf{P}} = \frac{\partial \Psi}{\partial \mathbf{E}} = (\bar{\mu} + \bar{\alpha})\mathbf{E} + (\bar{\mu} - \bar{\alpha})\mathbf{E}^T + \bar{\lambda} tr(\mathbf{E})\mathbf{I} \tag{11}$$

$$\bar{\mathbf{M}} = \frac{\partial \Psi}{\partial \bar{\mathbf{\Gamma}}} = (\bar{\gamma} + \bar{\kappa})\bar{\mathbf{\Gamma}} + (\bar{\gamma} - \bar{\kappa})\bar{\mathbf{\Gamma}}^T + \bar{\beta} tr(\bar{\mathbf{\Gamma}})\mathbf{I} \tag{12}$$

where $\bar{\mu}$ and $\bar{\lambda}$ are the Lamé parameters. $\bar{\alpha}, \bar{\beta}, \bar{\gamma}$, and $\bar{\kappa}$ are micropolar material parameters which can be correlated with measurable properties, e.g., shear modulus (G), coupling number (N), Poisson's ratio (ν), polar ratio (Φ), and the characteristics length for torsion (l_t) and bending (l_b) as

$$\bar{\mu} = G, \bar{\alpha} = \frac{GN^2}{1-N^2}, \bar{\lambda} = \frac{2\nu G}{1-2\nu}, \bar{\gamma} = G l_t^2, \bar{\kappa} = G(4l_b^2 - l_t^2), \bar{\beta} = \frac{2G l_t^2 (1-\Phi)}{\Phi} \tag{13}$$

Here, N, a unitless quantity, signifies the extent of interaction between the displacement and rotation fields. Characteristic lengths (l_b and l_t), quantify the effect of microstructure on macroscopic behavior. Using the relation $\mathbf{P} = \mathbf{Q}\bar{\mathbf{P}}$ and $\mathbf{M} = \mathbf{Q}\bar{\mathbf{M}}$, the constitutive equations (Eqs. (11) and (12)) can be used in the correspondence relations mentioned in Eqs. (9) and (10). Strain and wryness measures are given as (Sajal and Roy [7])

$$\mathbf{E} = \mathbf{Q}^T\mathbf{F} - \mathbf{I} \tag{14}$$

$$\bar{\mathbf{\Gamma}} = -\frac{1}{2}\mathbf{Q}^T(\boldsymbol{\varepsilon}: (\nabla \mathbf{Q}\mathbf{Q}^T)) \tag{15}$$

where $\mathbf{Q}$ is the rotation tensor.

3 NUMERICAL IMPLEMENTATION

3.1 Quasi-static formulation

Assuming the inertial terms to be zero and substituting the force density and couple stress density vector states, the governing equations (Eqs. (7) and (8)) can be written for a material point as follows:

$$\int_{H_\mathbf{x}} (\mathbf{Q}\bar{\mathbf{P}}\mathbf{g} - \mathbf{Q}'\bar{\mathbf{P}}'\mathbf{g}')dV' + \mathbf{b} = \mathbf{0} \tag{16}$$

$$\int_{H_\mathbf{x}} (\mathbf{Q}\bar{\mathbf{M}}\mathbf{g} - \mathbf{Q}'\bar{\mathbf{M}}'\mathbf{g}')dV' - \int_{H_\mathbf{x}} (\mathbf{y} - \mathbf{y}') \times (\mathbf{Q}\bar{\mathbf{P}}\mathbf{g})dV' + \mathbf{l} = \mathbf{0} \tag{17}$$

Eqs. (16) and (17) can be discretized and written for all the material points in the body. The solution for the set of nonlinear algebraic equation is determined using the Newton-Raphson method by checking the convergence at every load step. Assume that convergence is established in load step k. At this step, the deformed position vector and rotation tensor fields are represented by $\mathbf{y}^k$ and $\mathbf{Q}^k$, respectively. The residual vectors can be given as

$$\mathbf{R}_f(\mathbf{y}^k, \mathbf{Q}^k) = \int_{H_\mathbf{x}} (\mathbf{Q}\bar{\mathbf{P}}\mathbf{g} - \mathbf{Q}'\bar{\mathbf{P}}'\mathbf{g}')^k dV' + \mathbf{b}^k = \mathbf{0} \tag{18}$$

$$\mathbf{R}_m(\mathbf{y}^k, \mathbf{Q}^k) = \int_{H_\mathbf{x}} (\mathbf{Q}\bar{\mathbf{M}}\mathbf{g} - \mathbf{Q}'\bar{\mathbf{M}}'\mathbf{g}')^k dV' - \int_{H_\mathbf{x}} (\mathbf{y} - \mathbf{y}')^k \times (\mathbf{Q}\bar{\mathbf{P}}\mathbf{g})^k dV' + \mathbf{l}^k = \mathbf{0} \tag{19}$$

We assume a trial solution of $\mathbf{y}$ and $\mathbf{Q}$ for (k + 1)-th load step as $\mathbf{y}^{k+1,trial} = \mathbf{y}^k + \mathbf{v}^k$ and $\mathbf{Q}^{k+1,trial} = exp(\Delta\boldsymbol{\Theta}^{k,trial})\mathbf{Q}^k$, respectively. Here $\mathbf{v}^k$ and $\Delta\boldsymbol{\Theta}^{k,trial}$ are trial incremental displacement vector and rotation skew-symmetric tensor, respectively. As $\mathbf{y}^{k+1,trial}$ and $\mathbf{Q}^{k+1,trial}$ do not satisfy Eqs. (18) and (19) in general, we need to apply corrections to the trial solutions as

$$\mathbf{y}^{k+1} = \mathbf{y}^{k+1,trial} + \Delta\mathbf{v} \tag{20}$$

$$\mathbf{Q}^{k+1} = exp(\Delta\boldsymbol{\Theta})\mathbf{Q}^{k+1,trial} \tag{21}$$

Here $\Delta\mathbf{v}$ and $\Delta\boldsymbol{\Theta}$ represent the incremental displacement and small rotation tensor, respectively. $\Delta\mathbf{v}$ and $\Delta\boldsymbol{\Theta}$ are determined from the condition that $\mathbf{R}_f(\mathbf{y}^{k+1}, \mathbf{Q}^{k+1}) = \mathbf{0}$ and $\mathbf{R}_m(\mathbf{y}^{k+1}, \mathbf{Q}^{k+1}) = \mathbf{0}$. Expanding them using the Taylor series about the trial solution and neglecting the higher order terms leads to

$$\mathbf{R}_f(\mathbf{y}^{k+1}, \mathbf{Q}^{k+1}) = \mathbf{R}_f(\mathbf{y}^{k+1,trial}, \mathbf{Q}^{k+1,trial}) + \Delta\mathbf{R}_f = \mathbf{0} \tag{22}$$

$$\mathbf{R}_m(\mathbf{y}^{k+1}, \mathbf{Q}^{k+1}) = \mathbf{R}_m(\boldsymbol{y}^{k+1,trial}, \mathbf{Q}^{k+1,trial}) + \Delta\mathbf{R}_m = \mathbf{0} \tag{23}$$

Here change of $\boldsymbol{R_f}$and $\boldsymbol{R}_m$ can be calculated as

$$\Delta\mathbf{R}_f = \int_{H_\mathbf{x}} (\Delta\boldsymbol{\Theta}\mathbf{Q}\bar{\mathbf{P}}\mathbf{g} + \mathbf{Q}\frac{\partial\bar{\mathbf{P}}}{\partial\mathbf{E}}\mathbf{Q}^T(\nabla(\Delta\mathbf{v}) - \Delta\boldsymbol{\Theta}\mathbf{F})\mathbf{g} - \Delta\boldsymbol{\Theta}'\mathbf{Q}'\bar{\mathbf{P}}'\mathbf{g}' - \mathbf{Q}'\frac{\partial\bar{\mathbf{P}}'}{\partial\mathbf{E}}\mathbf{Q}'^T(\nabla(\Delta\mathbf{v}') - \Delta\boldsymbol{\Theta}'\mathbf{F}')\mathbf{g}')^k dV' + \Delta\mathbf{b}^k \tag{24}$$

$$\Delta\mathbf{R}_m = \int_{H_\mathbf{x}} \left[\Delta\boldsymbol{\Theta}\mathbf{Q}\bar{\mathbf{M}}\mathbf{g} + \mathbf{Q}\frac{\partial\bar{\mathbf{M}}}{\partial\bar{\boldsymbol{\Gamma}}}\mathbf{Q}^T\nabla(\Delta\boldsymbol{\theta})\mathbf{g} - \Delta\boldsymbol{\Theta}'\mathbf{Q}'\bar{\mathbf{M}}'\mathbf{g}' + \mathbf{Q}'\frac{\partial\bar{\mathbf{M}}'}{\partial\bar{\boldsymbol{\Gamma}}'}\mathbf{Q}'^T\nabla(\Delta\boldsymbol{\theta}')\mathbf{g}'\right]^k dV' + \int_{H_\mathbf{x}} \left[(\Delta\mathbf{v} - \Delta\mathbf{v}') \times \mathbf{Q}\bar{\mathbf{P}}\mathbf{g} + (\mathbf{y} - \mathbf{y}') \times \left(\Delta\boldsymbol{\Theta}\mathbf{Q}\bar{\mathbf{P}}\mathbf{g} + \mathbf{Q}\frac{\partial\bar{\mathbf{P}}}{\partial\mathbf{E}}\mathbf{Q}^T(\nabla(\Delta\mathbf{v}) - \Delta\boldsymbol{\Theta}\mathbf{F})\mathbf{g}\right)\right]^k dV' + \Delta\mathbf{l}^k \tag{25}$$

3.2 Dynamic formulation

The numerical solution of the governing micropolar PD equations is determined by employing the Newmark-beta method. Convergence at every time step is ensured by employing the Newton-Raphson method. Newmark-beta time integration parameters γ and β are chosen as 1/2 and 1/6, respectively, which corresponds to the linear acceleration method. The linearized governing equations are obtained as follows:

$$\left(\frac{6\rho}{\Delta t^2}\mathbf{I} + \frac{\partial\mathbf{R}_f}{\partial\mathbf{y}}\Big|_{(\mathbf{y}_i + \Delta\mathbf{y}_i^n,\ exp(\Delta\boldsymbol{\Theta}_i^n)\mathbf{Q}_i)}\right)\delta\Delta\mathbf{y}_i + \frac{\partial\mathbf{R}_f}{\partial\theta}\Big|_{(\mathbf{y}_i + \Delta\mathbf{y}_i^n,\ exp(\Delta\boldsymbol{\Theta}_i^n)\mathbf{Q}_i)}\delta\Delta\boldsymbol{\theta}_i = \Delta\mathbf{b}_i - (\Delta\mathbf{R}_f)_i^n + \frac{6\rho}{\Delta t}\dot{\mathbf{y}}_i + 3\rho\ddot{\mathbf{y}}_i - \frac{6\rho}{\Delta t^2}\Delta\mathbf{y}_i^n \tag{26}$$

$$\left(\frac{6I_p}{\Delta t^2}+\left.\frac{\partial \mathbf{R}_m}{\partial \boldsymbol{\theta}}\right|_{(\mathbf{y}_i+\Delta\mathbf{y}_i^n,\ exp(\Delta\boldsymbol{\Theta}_i^n)\mathbf{Q}_i)}\right)\delta\Delta\boldsymbol{\theta}_i+\left.\frac{\partial R_m}{\partial \mathbf{y}}\right|_{(\mathbf{y}_i+\Delta\mathbf{y}_i^n,\ exp(\Delta\boldsymbol{\Theta}_i^n)\mathbf{Q}_i)}\cdot\delta\Delta\mathbf{y}_i=\Delta\mathbf{l}_i-(\Delta R_m)_i^n+\frac{6I_p}{\Delta t}\dot{\boldsymbol{\theta}}_i+3I_p\ddot{\boldsymbol{\theta}}_i-\frac{6I_p}{\Delta t^2}\Delta\boldsymbol{\theta}_i^n \tag{27}$$

where $\mathbf{R}_f=\int_{H_\mathbf{x}}(\mathbf{T}-\mathbf{T}')dV'$ and $\mathbf{R}_m=\int_{H_\mathbf{x}}(\mathbf{m}-\mathbf{m}')dV'-\int_{H_\mathbf{x}}(\mathbf{y}-\mathbf{y}')\times\mathbf{T}dV'+\mathbf{w}\times(\mathbf{I}_p\mathbf{w})$. **I** represent the identity matrix and Δt is the time step. Eqs. (26) and (27) can be written for all the material points and solved for $\delta\Delta\mathbf{y}_i$ and $\delta\Delta\boldsymbol{\theta}_i$ for all particles after applying the boundary conditions. Once $\delta\Delta\mathbf{y}_i$ and $\delta\Delta\boldsymbol{\theta}_i$ are calculated, $\Delta\mathbf{y}_i^{n+1}$ and $\Delta\mathbf{Q}_i^{n+1}$ can be determined as follows:

$$\Delta\mathbf{y}_i^{n+1}=\Delta\mathbf{y}_i^n+\delta\Delta\mathbf{y}_i \tag{28}$$

$$\Delta\mathbf{Q}_i^{n+1}=\exp(\delta\Delta\boldsymbol{\Theta}_i)\exp(\Delta\boldsymbol{\Theta}_i^n) \tag{29}$$

The deformation and rotation of a point can be calculated as

$$\mathbf{y}_i^{n+1}=\mathbf{y}_i+\Delta\mathbf{y}_i^{n+1} \tag{30}$$

$$\mathbf{Q}_i^{n+1}=\exp(\Delta\mathbf{Q}_i^{n+1})\mathbf{Q}_i \tag{31}$$

4 NUMERICAL SIMULATIONS

4.1 Plate with hole

Validation of the proposed micropolar PD theory is carried out by analyzing a plate having a circular hole of radius (r) of 0.5 mm at the center under tensile loading and comparing the stress concentration with solution derived from boundary element method (BEM). The BEM solution is based on Eringen's micropolar elasticity theory given by Huang and Liang [9]. Due to symmetry in geometry and loading condition, only one quadrant of the plate discretized into 639677 material points is analyzed as shown in Figure 2a. The material parameters are borrowed from Huang and Liang [9]. The specimen is subjected to uniform tensile stress (σ_0) of 1000 N/m^2. Stress concentration along the *x*-axis is determined by computing the ratio of stress along the *x*-axis (σ_{xx}) to the applied stress σ_0. Variation of the stress concentration along the *y*-axis, as depicted in Figure 2b, shows close agreement between the micropolar PD and BEM solution. This demonstrates the effectiveness of the proposed micropolar PD model.

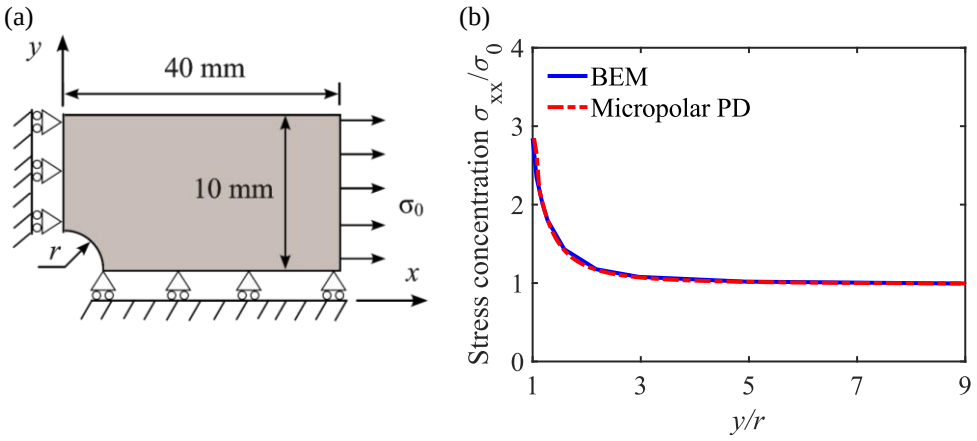

Figure 2. One quadrant of the plate with a circular hole at center: (a) geometry with boundary conditions, (b) stress concentration along the *y*-axis.

4.2 Periodic cellular metamaterial

Two periodic cellular metamaterials with 10×10 circular holes of diameter 8.67 mm and made up of styrene-butadiene rubber (SBR) having E = 7780.6 kPa and ν = 0.4516 are considered in this section. A displacement controlled compressive load in vertical direction is applied on the top edge keeping the bottom edge fixed. Geometrical perturbation is provided to the holes along mode 1 deformation pattern to induce instability [2]. Plane strain condition is assumed in both nonpolar PD and micropolar PD. Neo-Hookean constitutive model is used for nonpolar NOSB-PD formulation to capture moderately large deformation.

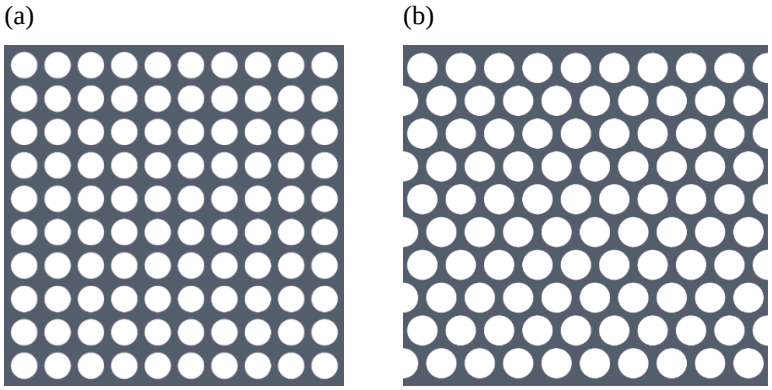

Figure 3. Reference configurations: (a) Configuration 1, (b) Configuration 2.

First, the effect of the micropolar material parameters on nominal stress vs. nominal strain response are examined through Configuration 1 as shown in Figure 3a. The specimen is 101 mm in height and width with holes positioned at distance of 9.97 mm center-to-center, along both horizontal and vertical directions. Center of the nearest hole from the edges of the specimen is at 5.64 mm. Each hole is perturbed by 1.44% of its original hole radius. The specimen is discretized uniformly into 67921 material points. Five distinct cases with different micropolar constants, mentioned in Table 1, are considered. For the two-dimensional analysis,

Φ = 1 and $l_t = \sqrt{2}l_b$. It can be noted from the variation of nominal stress with nominal strain shown in Figure 4 that the increase or decrease in $\bar{\kappa}$ and $\bar{\alpha}$ values directly correspond to increase or decrease in the critical load at which buckling occurs, respectively. From the nominal stress vs. strain curves of Cases 1 to 3 in which $\bar{\kappa}$ is same and $\bar{\alpha}$ is varied, it can be observed that increasing the $\bar{\alpha}$ value decreases the critical load by small amount. Similarly, from the nominal stress vs. strain curves of Cases 3 to 5 in which $\bar{\alpha}$ is same and $\bar{\kappa}$ is varied, it can be observed that the critical load increase significantly with increase in the $\bar{\kappa}$ value. The change in $\bar{\kappa}$ value considerably influences the critical load in comparison to the $\bar{\alpha}$ value. The $\bar{\kappa}$ and $\bar{\alpha}$ values can be determined by calibrating the response with the experimental results.

Table 1. Micropolar constants for different cases

Case/Micropolar constants	$\bar{\alpha}$	$\bar{\kappa}$
Case 1	$G/2$	$G/(14\times10^6)$
Case 2	$G/32$	$G/(14\times10^6)$
Case 3	$G/8$	$G/(14\times10^6)$
Case 4	$G/8$	$G/(21\times10^6)$
Case 5	$G/8$	$G/(7\times10^6)$

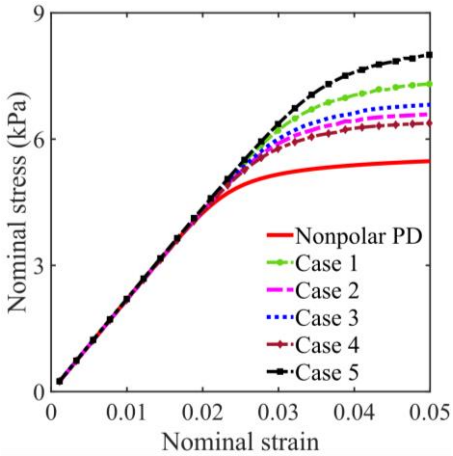

Figure 4. Variation of nominal stress with nominal strain in Configuration 1 with different micropolar parameters.

In the subsequent simulation, $\bar{\alpha} = G/8$ and $\bar{\kappa} = G/(14\times10^6)$ are considered for SBR material for further investigations. The deformation response is further analyzed with the specified micropolar constants for both metamaterials, i.e., Configuration 1 and Configuration 2. In Configuration 2 of height 98.5 mm and width 104.3 mm, circular holes perturbed by 1.33% of original hole radius are positioned at spacing of 10.97 mm and 9.47 mm center-to-center along horizontal and vertical directions, respectively. Center of first hole from both top and left side are kept at 6.64 mm and 5.53 mm from top and bottom edge distances, respectively, shown in Figure 3b. The specimen is discretized uniformly into 85682 material points.

Nominal stress vs. nominal strain curves obtained using micropolar PD and nonpolar PD models are depicted in Figure 5. The significant difference between micropolar PD and nonpolar PD result illustrates the effect of micropolarity on the initiation of local instability. The displacement and rotation contours of Configuration 1 are presented in Figs. 6a, 6b, and 6c. It can be observed that holes transform into mutually orthogonal ovals under critical loading. Rotation of the particles is considerably higher near the completely transformed oval near the central region of the specimen than the loading and support edges as shown in Figure 6c. In Configuration 2, holes transform into inclined oval shaped holes with alternate orientations in row as shown in Figs. 6d, 6e, and 6f. This pattern transformation results in clockwise and anticlockwise rotations in the alternate layers of holes which is shown in the rotation contour furnished in Figure 6f. The presence of large rotation near transformed holes demonstrates the need for finite deformation micropolar PD theory.

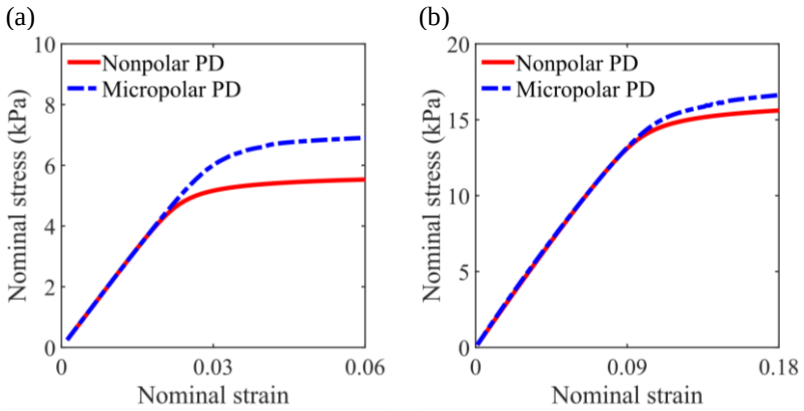

Figure 5. Comparison of nominal stress vs. nominal strain variation between micropolar PD with nonpolar PD solution: (a) Configuration 1, (b) Configuration 2.

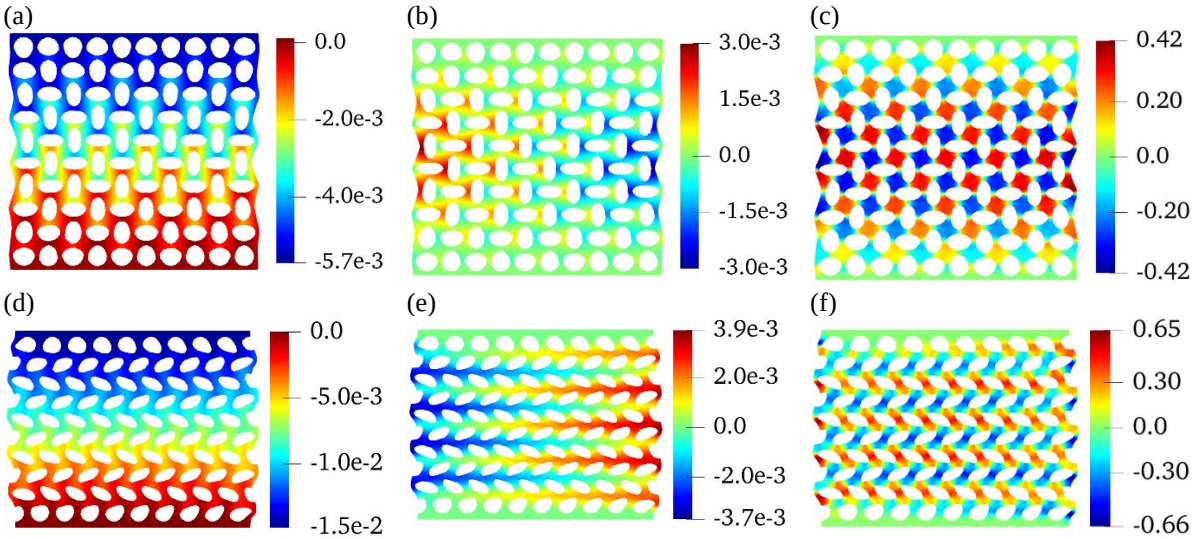

Figure 6. Displacement contour (m) and rotation contour (radian) plots: Configuration 1 at strain 0.05 (a) vertical displacement, (b) horizontal displacement, (c) rotation; Configuration 2 at strain 0.15 (d) vertical displacement, (e) horizontal displacement, (f) rotation.

4.2 Dynamic simulation

This section presents wave propagation through metamaterials with periodic arrangement of cracks and holes and assesses the effect of micropolarity assuming plane strain condition. All the specimens are made of SBR material of density 980 kg/m^3. The mass moment of inertia density of each PD particles is considered 12.25×10^{-3} kg/m. The left edge of the specimen is considered fixed and a compressive force of 200 N is applied on the right edge.

Configuration 1 comprises of 25 cracks of 6 mm length and placed at spacing of 6 mm along vertical and horizontal directions. The cracks are placed such that adjacent cracks are orthogonal to each other and the distance of top and right edges of the specimen from the center of nearest cracks is 5.61 mm as shown in Figure 7a. The specimen is discretized uniformly into 43755 PD particles. Configuration 2 comprises of 5×5 elliptical holes of major and minor axes length of 5 mm and 3 mm, respectively. The elliptical holes are placed such that the major axis of adjacent elliptical holes is orthogonal to each other as shown in Figure 7b. The specimen is discretized uniformly into 32488 PD particles. Configuration 3 comprises of 5×5 circular holes of diameter 5 mm as shown in Figure 7c. The specimen is discretized into 31724 PD particles. In Configurations 2 and 3, holes are placed at a spacing of 6 mm maintaining a distance of 5.61 mm between the top and right edges from the center of nearest holes.

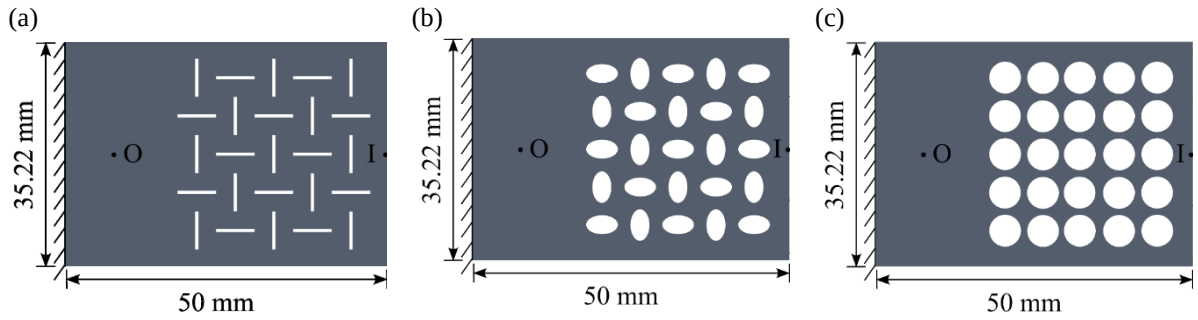

Figure 7. Metamaterial specimen: (a) Configuration 1, (b) Configuration 2, (c) Configuration 3.

Figure 8 presents the time history of horizontal displacement at point O obtained using micropolar PD and nonpolar PD. The difference in response obtained from micropolar PD and nonpolar PD demonstrates the importance of incorporation of micropolar theory in PD formulation.

Figure 9 furnishes the rotation contour plots of Configuration 1 at 2 ms, 4 ms, and 5 ms. From the rotation contours, it can be observed that the solid regions enclosed by the cracks experience considerable rotation. The rotation contour plots of Configuration 2 and Configuration 3 are shown in Figs. 9d to 9f and Figs. 9g to 9i, respectively, at 1 ms, 2 ms, and 3 ms. The regions enclosed by the holes undergo a significant rotation. As large localized rotation occurs in the regions surrounded by the cracks and holes, and classical theory may underestimate the amount of rotation, micropolar PD model is used.

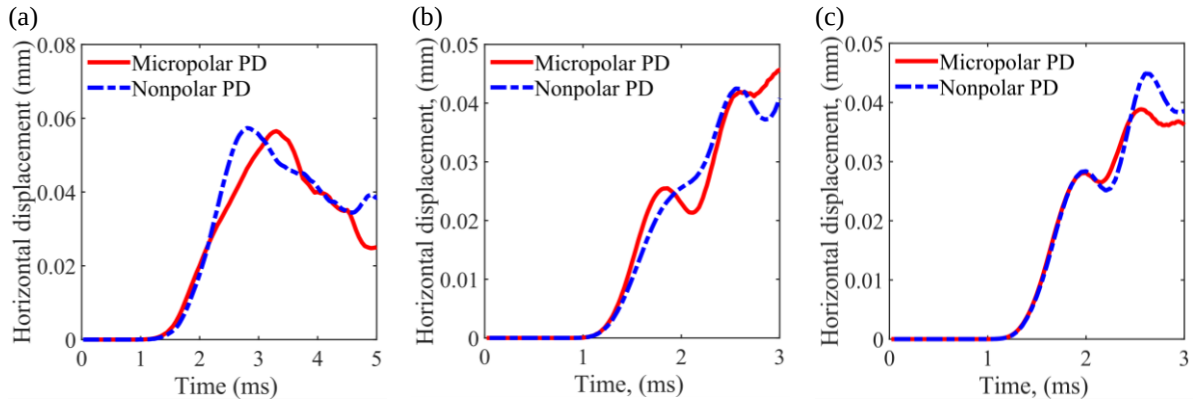

Figure 8. Horizontal displacement time history at point O: (a) Configuration 1, (b) Configuration 2, (c) Configuration 3.

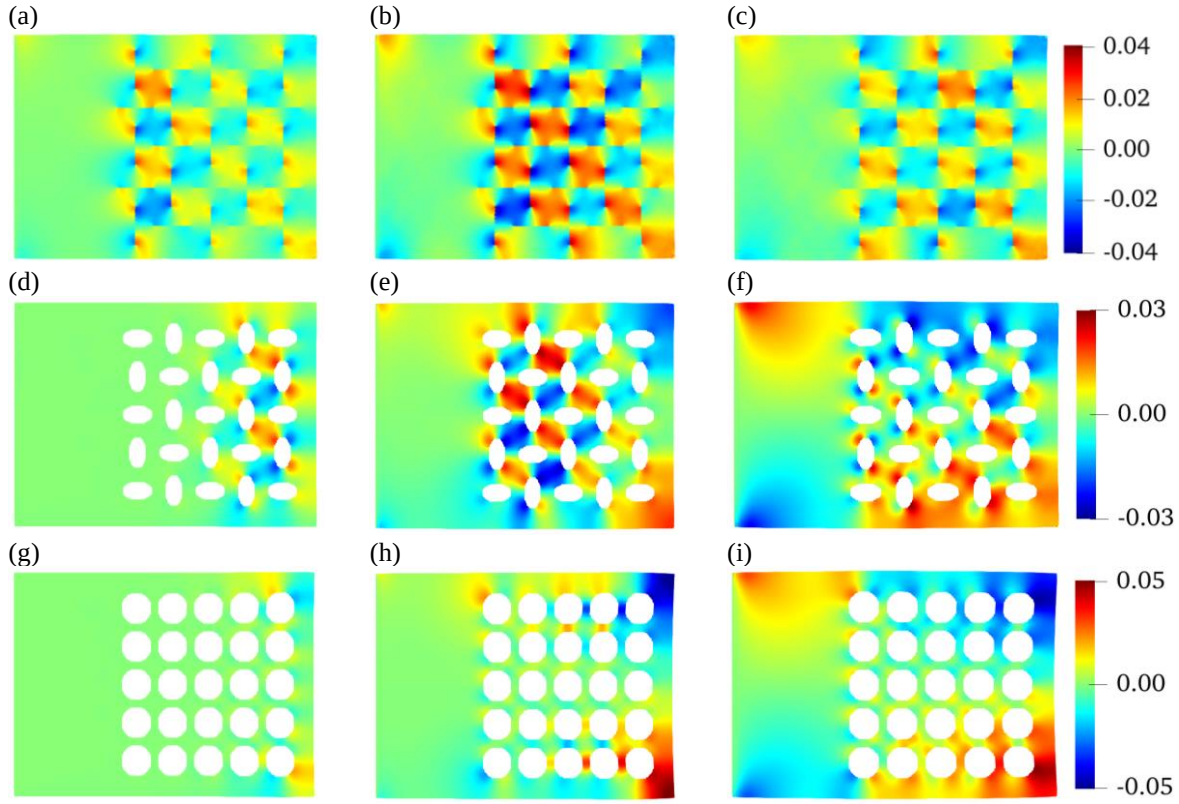

Figure 9. Rotation contour (radian): Configuration 1 at (a) 2 ms, (b) 4 ms, (c) 5 ms; Configuration 2 at (d) 1 ms, (e) 2 ms, (f) 3 ms; Configuration 3 at (g) 1 ms, (h) 2 ms, (i) 3 ms.

5 CONCLUSIONS

We present a micropolar PD theory for large deformation, incorporating an additional governing equation of motion. First, the PD model is validated by showing close agreement in stress concentration variation with BEM solution. Next, periodic cellular structures consisting of holes are examined and the influence of micropolar parameters on the response is investigated. It is observed that the micropolar parameters $\bar{\kappa}$ and $\bar{\alpha}$ directly influence the slope

of normal stress vs. strain curve and the critical load at which buckling occurs. Finally, the wave propagation through periodic metamaterial with cracks and holes is examined. A significant amount of rotation is observed near the area surrounded by the cracks and holes during the wave propagation which demonstrates the applicability of micropolar theory.

REFERENCES

[1] Golub, M.V. Zhang, C. and Wang, Y. S. SH-wave propagation and scattering in periodically layered composites with a damaged layer, *J Sound Vib*. (2012), **331**:1829-1843.

[2] Sajal and Roy, P. Peridynamics modeling of cellular elastomeric metamaterials: application to wave isolation, *Int. J. Mech. Sci.* (2023) **254**:108456.

[3] Pietraszkiewicz, W. and Eremeyev, V.A. On natural strain measures of the non-linear micropolar continuum, *Int J Solids Struct*. (2009) **46**:774–787.

[4] Silling, S.A. Reformulation of elasticity theory for discontinuities and long-range forces, *J. Mech. Phys. Solids*. (2000), **48**:175-209.

[5] Silling, S.A. Epton, M. Weckner, O. Xu, J. and Askari, E. Peridynamic states and constitutive modeling, *J Elast*. (2007), **88**:151-184.

[6] Chen, H. and Spencer, B.W. Peridynamic bond-associated correspondence model: stability and convergence properties, *Int J Numer Methods Eng*. (2019), **117**:713-727.

[7] Sajal and Roy, P. Finite deformation micropolar peridynamic theory: Variational consistency of wryness measure, *Int. J. Mech. Sci.* (2024) **271**:109306.

[8] W. Nowacki, Theory of Asymmetric Elasticity, Pergamon Press, 1986.

[9] Huang, F.Y. and Liang, K.Z. Boundary element analysis of stress concentration in micropolar elastic plate, *Int. J. Numer. Methods Eng.* (1997), **40**:1611-1622.